Front. Phys. 13(5), 130508 (2018)
https://doi.org/10.1007/s11467-018-0805-0

RESEARCH ARTICLE

Cross and joint ordinal partition transition networks for multivariate time series analysis

Heng Guo, Jia-Yang Zhang, Yong Zou†, Shu-Guang Guan‡

Department of Physics, East China Normal University, Shanghai 200062, China
Corresponding authors. E-mail: †yzou@phy.ecnu.edu.cn, ‡sgguan@phy.ecnu.edu.cn
Received April 16, 2018; accepted May 25, 2018

We propose the construction of cross and joint ordinal pattern transition networks from multivariate time series for two coupled systems, where synchronizations are often present. In particular, we focus on phase synchronization, which is a prototypical scenario in dynamical systems. We systematically show that cross and joint ordinal pattern transition networks are sensitive to phase synchronization. Furthermore, we find that some particular missing ordinal patterns play crucial roles in forming the detailed structures in the parameter space, whereas the calculations of permutation entropy measures often do not. We conclude that cross and joint ordinal partition transition network approaches provide complementary insights into the traditional symbolic analysis of synchronization transitions.

Keywords nonlinear time series analysis, complex networks, ordinal pattern partition, transition network, phase synchronization

PACS numbers 05.45.Ac, 89.75.Fb, 05.45.Tp

1 Introduction

Complex network theory provides an important paradigm for understanding the structural properties of complex systems composed of different interacting entities. During the previous decade, various complex network approaches have been proposed to extract useful insights from time series data [1]. Depending on slightly different definitions of nodes and links of network representations for time series, there are methods based on recurrences [2, 3], visibility conditions [4], cycle detections [5], and correlation networks [6]. Some successful applications of these methods include time series from climate changes, sunspots, oil–water flows, and financial markets [1, 7–16]. The consideration of a time series as a complex network allows a reinterpretation of many network theoretic measures in terms of the characteristic phase space properties of a dynamical system [17].

Recently, a growing number of works have focused on transforming time series into networks by ordinal partitions of the time series [18–22]. The basic idea of the ordinal partition network method can be traced back to identifying ordinal patterns of time series [23–25]. Given a one-dimensional time series $\{x(t)\}_{t=1,\cdots,L}$ comprising L points from a dynamical system, we first reconstruct its phase space by a time delay embedding technique, which yields $\boldsymbol{x}(t) = [x(t), x(t+\tau), \cdots, x(t+(D_x-1)\tau)]$, where D_x and τ are the embedding dimension and delay, respectively [26, 27]. The next step is to compute the rank order of each embedded vector $[x(t), x(t+\tau), \cdots, x(t+(D_x-1)\tau)]$, which is conveniently denoted by a symbol $\pi_x(t)$. When sliding windows from $t = 1$ to $N = L-(D_x-1)\tau$ in the embedded space, a symbolic representation of the trajectory $\pi_x(t)$ is produced. Following the symbolic representation, one traditional approach is to compute the permutation entropy $\mathcal{H}_O$ based on the frequency plot of order patterns. Generally speaking, for a time series generated by a stochastic process for $N \to \infty$, it is known that all $D_x!$ patterns occur with almost equal probabilities, which yields the maximal value of $\mathcal{H}_O$. However, for a time series produced by deterministic dynamics, the frequency plot of the $D_x!$ patterns is not uniform, which leads to a reduced value of $\mathcal{H}_O$. In some cases, a set of patterns may never occur, and these missing patterns are often called forbidden patterns; these patterns provide important information for quantifying determinism in time series data [28–32]. Next, the level of determinism of a time series from a particular dynamical system may be suggested by the permutation entropy $\mathcal{H}_O$, which consists of very well-established statistical measures in nonlinear time se-

*arXiv: 1806.01724.

ries analysis [23, 25, 33]. Some applications include characterizations of the difference between healthy and sick patients from EEG data [18, 19]. It is worth noting that complications may arise in real time analysis because missing ordinal patterns might be related to a finite time length during the period of observation and correlated stochastic processes, which require some revised methods for the detection of determinism in relatively short noisy data [28–32].

The primary idea of an ordinal partition transition network takes into account the inhomogeneous evolutionary behavior among the ordinal patterns [18, 19], which provides complementary information on the standard ordinal symbolic analysis of time series. Most previous works have focused on univariate time series $\{x(t)\}$. The embedding parameters D_x and τ have crucial impacts on the resulting ordinal partition transition networks, especially for forbidden patterns [20–22]. In addition, multivariate time series are ubiquitous in nature, ranging from stock markets to climate science. In a recent work, we proposed to construct ordinal partition transition networks from multivariate data [34]. The resulting network is a directed and weighted network characterizing the pattern transition properties of time series in its associated velocity space. This novel approach has been successfully applied to capture phase coherence to non-phase coherence transitions and to characterize paths to phase synchronization, showing complementary insight to the traditional symbolic analysis of nonlinear time series analysis.

In this work, we further extend these ideas [34] to construct cross and joint ordinal partition transition networks for two coupled systems. We show that both cross and joint ordinal pattern transition networks are able to capture synchronization transitions, in particular, focusing on the transitions to phase synchronization (PS), which is one of the paradigmatic types of synchronization phenomena [35–40]. The outline of this paper is as follows: first, we illustrate cross and joint network construction approaches, and we then introduce two entropy measures to quantify the inhomogeneous frequencies of ordinal patterns and their transitions in Section 2. We apply these two entropy measures to characterize the synchronization transitions with both unidirectional and bidirectional coupling schemes in Section 3, and then some conclusions are drawn in Section 4.

2 Cross and joint ordinal partition transition networks

2.1 Network constructions

The ordinal partition transition networks are illustrated by the following coupled Rössler systems [41, 42], which shows transition scenarios to phase synchronization for various coupling schemes. In particular, PS has been observed for both unidirectional and bidirectional couplings. Note that the network construction method is not restricted by the following model. The ordinary differential equations (ODEs) of the coupled system read

$$\begin{cases} \dot{x}_1 = -(1.0-\Delta)y_1 - z_1 + \kappa_1(x_2 - x_1), \\ \dot{y}_1 = (1.0-\Delta)x_1 + 0.15y_1, \\ \dot{z}_1 = 0.2 + z_1(x_1 - 10.0), \end{cases}$$

$$\begin{cases} \dot{x}_2 = -(1.0+\Delta)y_2 - z_2 + \kappa_2(x_1 - x_2), \\ \dot{y}_2 = (1.0+\Delta)x_2 + 0.15y_2, \\ \dot{z}_2 = 0.2 + z_2(x_2 - 10.0), \end{cases}$$

where $\omega_1 = 1.0 - \Delta$, $\omega_2 = 1.0 + \Delta$ are frequencies for the systems and $\kappa_{1,2}$ are the coupling strengths. In this model, we distinguish a unidirectional coupling case from a bidirectional coupling one because the threshold values to PS have been reported in the literature [41, 42]. More specifically the unidirectional coupling can be achieved by $\kappa_1 = 0$, i.e., a drive-response scheme [41], and bidirectional coupling is often chosen as $\kappa_1 = \kappa_2 = \kappa$ [42]. We numerically integrate the ODEs using the fourth-order Runge-Kutta method with random initial conditions and the integration step $h = 0.01$. The first 10000 transient data points are discarded, and time series consisting of $N = 800000$ data points are analyzed.

Ordinal pattern transition network. We begin by constructing the ordinal pattern transition network for a single system, using the first system [Eqs. (1), $\omega_1 = 1.0$, $\Delta = 0$, $\kappa_{1,2} = 0$] as an example [34]. Given time series $(x(t), y(t), z(t))$ in the corresponding three-dimensional phase space ($n = 3$), the ordinal pattern transition network is reconstructed based on the signs of the increments of each variable $(\Delta x(t), \Delta y(t), \Delta z(t))$, where $\Delta x(t) = x(t+1) - x(t)$, $\Delta y(t) = y(t+1) - y(t)$, and $\Delta z(t) = z(t+1) - z(t)$. In particular, the definitions of the ordinal patterns based on the increment series capture the variations of the trajectory in its associated velocity space. The definition of patterns $\Pi(t) \in (\pi_1, \cdots, \pi_i), i = 1, \cdots, 8$ are enumerated in Table 1. As time passes, the transition behavior between patterns is illustrated in Fig. 1(a). The deterministic transitions are explained by the ordinal partitions of phase space by null-clines. A transition between two patterns means the trajectory crosses a null-cline, which leads to a local maximum or minimum. Because of the continuity of the system in phase space, we only observe the transition route $\pi_1 \to \pi_5 \to \pi_6 \to \pi_8 \to \pi_4 \to \pi_3 \to \pi_1$, yielding two missing patterns, π_2 and π_7, as shown in Fig. 1(a). These details have been illustrated in Ref. [34].

Generalizing the above ideas from a single system to two coupled systems ($\kappa_{1,2} \neq 0$), we propose two different methods to construct ordinal pattern transition networks. Suppose we have time series $(x_1(t), y_1(t), z_1(t))$ of

Table 1 Definitions of ordinal patterns of the three-dimensional time series $(x(t), y(t), z(t))$, where $\Delta x = x(t+1) - x(t)$, $\Delta y = y(t+1) - y(t)$, and $\Delta z = z(t+1) - z(t)$ [34].

Π	π_1	π_2	π_3	π_4	π_5	π_6	π_7	π_8
Δx	+	+	+	+	−	−	−	−
Δy	+	+	−	−	+	+	−	−
Δz	+	−	+	−	+	−	+	−

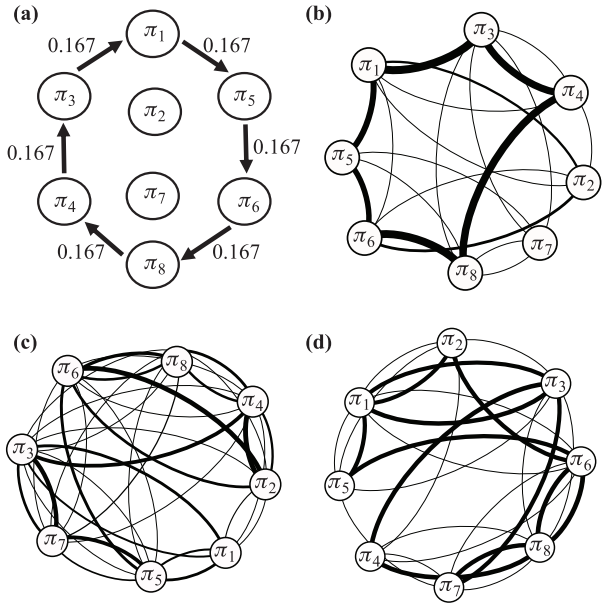

Fig. 1 Ordinal pattern transition network, where the thickness (and values) of network links represent the corresponding transition frequency between two patterns. **(a)** A single chaotic Rössler system. **(b)** Cross ordinal pattern transition network (COPT) for two coupled Rössler systems, **(c)** an alternative version of COPT, and **(d)** joint ordinal pattern transition network (JOPT). For (b)–(d), the directions of links have been suppressed for better visualization. In addition, the coupling strength $\kappa_{1,2}$ is in the non-sync regime, i.e., $\kappa_1 = 0$, $\kappa_2 = 0.01$.

one system and $(x_2(t), y_2(t), z_2(t))$ of the other; we first compute the respective increments of the two systems as $(\Delta x_1(t), \Delta y_1(t), \Delta z_1(t))$ and $(\Delta x_2(t), \Delta y_2(t), \Delta z_2(t))$. Note that the increment series capture the dynamic properties of time series in the difference space, and the signs of the each variable reflect either an increasing (+) or decreasing (−) trend. Next, we compare the two systems.

Cross ordinal pattern transition network (COPT). A COPT compares the relative speeds between two systems by the signs of $(\Delta x_1(t) - \Delta x_2(t))$, $(\Delta y_1(t) - \Delta y_2(t))$ and $(\Delta z_1(t) - \Delta z_2(t))$. The pattern definitions of a COPT are shown in Table 2. An example of a COPT is shown in Fig. 1(b). In this work, we only consider the signs of the same variable from two coupled systems. A further generalization of the pattern definitions of a COPT is to consider the signs of cross-variables, for instance, $(\Delta x_1(t) - \Delta y_2(t))$ and $(\Delta x_1(t) - \Delta z_2(t))$, respectively. Considering the effects of the different magnitudes of the three variables, we also compute an *alternative* COPT by replacing $\Delta x_1(t) - \Delta x_2(t)$ by $\Delta x_1(t)/x_1(t) - \Delta x_2(t)/x_2(t)$, respectively, $\Delta y_1(t) - \Delta y_2(t)$ by $\Delta y_1(t)/y_1(t) - \Delta y_2(t)/y_2(t)$, and $\Delta z_1(t) - \Delta z_2(t)$ by $\Delta z_1(t)/z_1(t) - \Delta z_2(t)/z_2(t)$. An example of the alternative COPT is shown in Fig. 1(c). Comparing Fig. 1(b) to (c), the alternative COPT better reflects the non-coherent transitions between ordinal patterns because the coupling strength is in the non-synchronization regime ($\kappa_1 = 0$ and $\kappa_2 = 0.01$). In the following, we compute the alternative COPTs without distinguishing these two slightly different versions.

Joint ordinal pattern transition network (JOPT). A JOPT compares the relative speeds between two systems using the signs of $\Delta x_1(t) \cdot \Delta x_2(t)$, $\Delta y_1(t) \cdot \Delta y_2(t)$, and $\Delta z_1(t) \cdot \Delta z_2(t)$; the pattern definitions of a JOPT are summarized in Table 3. An example of a JOPT is shown in Fig. 1(d). In contrast to cross ordinal patterns, we notice that the joint ordinal patterns represent whether the respective variables of two systems show the same trend of changes or not, regardless of the magnitudes of the respective variables.

A direct quantitative comparison between a COPT and a JOPT does not seem possible because we have different definitions for patterns. Nevertheless, there are qualitative similarities when we show a COPT and a JOPT for two interacting stochastic processes in Fig. 2. In particular, we consider two stationary processes X_t and Y_t, each of which admits an autoregressive representation

$$X_t = \sum_{j=1}^{p} a_{2j} X_{t-j} + \sum_{j=1}^{p} b_{2j} Y_{t-j} + \eta_{1t}, \tag{1}$$

$$Y_t = \sum_{j=1}^{p} c_{2j} X_{t-j} + \sum_{j=1}^{p} d_{2j} Y_{t-j} + \eta_{2t}, \tag{2}$$

Table 2 Pattern definitions of a COPT. Note that "+" means a positive value, while "−" is for a negative value.

Π	π_1	π_2	π_3	π_4	π_5	π_6	π_7	π_8
$\Delta x_1 - \Delta x_2$	+	+	+	+	−	−	−	−
$\Delta y_1 - \Delta y_2$	+	+	−	−	+	+	−	−
$\Delta z_1 - \Delta z_2$	+	−	+	−	+	−	+	−

Table 3 Pattern definitions of a JOPT. Note that "+" means a positive value, while "−" is for a negative value.

Π	π_1	π_2	π_3	π_4	π_5	π_6	π_7	π_8
$\Delta x_1 \cdot \Delta x_2$	+	+	+	+	−	−	−	−
$\Delta y_1 \cdot \Delta y_2$	+	+	−	−	+	+	−	−
$\Delta z_1 \cdot \Delta z_2$	+	−	+	−	+	−	+	−

where the noise terms η_{1t}, η_{2t} are uncorrelated; p is the order; and a_{2j}, b_{2j}, c_{2j}, and d_{2j} are model coefficients. The terms of b_{2j} and c_{2j} reflect the interacting strength between X_t and Y_t; therefore, if X_t and Y_t are independent, b_{2j} and c_{2j} are uniformly zero. Here, we consider a simple case of $p = 2$, $a_{2j} = 0.5$, $b_{2j} = 0.1$, $c_{2j} = 0.5$, and $d_{2j} = 0$, when there are only unidirectional interactions from Y_t to X_t.

To maintain the same number of ordinal patterns as defined in Tables 2 and 3, we reconstruct a three-dimensional phase space for X_t (respectively Y_t) using time delay embedding techniques ($\tau = 1$). Figure 2(a) shows the ordinal pattern transition network for a single stochastic process, where we find rather random transition patterns in the resulting network. These random transitions between patterns have been observed in the COPT and JOPT [Figs. 2(b), (c) and (d)]. When increasing the interacting strength term b_{2j}, one would expect some reduced level of random pattern transitions in the X_t process because of the unidirectional interactions from the Y_t process. The dependence on the interaction strength requires further investigation and is beyond the scope of the current work.

2.2 Permutation entropy

In the next step, we quantify the heterogeneous properties of the resulting networks. For a deterministic system, the frequencies of ordinal patterns are generally different from each other, and the existence of forbidden patterns is simply a special case in this respect. Traditionally, the permutation entropy $\mathcal{H}$ is introduced to characterize the inhomogeneous appearance of ordinal patterns as follows

$$\mathcal{H}_O = -\sum_{i=1}^{2^n} p(\pi_i) \log_2 p(\pi_i), \tag{3}$$

where the sum runs over all $D = 2^n$ permutations, n is the dimension of one system, and $p(\pi_i)$ is the probability of order pattern π_i. We use the observation frequency $\mathcal{F}(\pi_i)$ to estimate $p(\pi_i)$ and also use $\log_2$; hence, the units of $\mathcal{H}_O$ are bits. For an n-dimensional independent identical distributed stochastic process, one obtains the largest entropy $\mathcal{H}_O = n$ because each of $D = 2^n$ ordinal patterns is expected to have the same frequency.

The computation of $\mathcal{H}_O$ characterizes the different frequencies of order patterns, and it has been well demonstrated that the transition behavior between ordinal patterns is not fully captured by $\mathcal{H}_O$ [34]. To this end, we first indicate each directed link representing the order pattern transitions in the resulting network by its transition frequency $w_{ij} = p(\pi_i \to \pi_j)$, following the time iterations of the series. To emphasize the importance of non-self transitions between ordinal patterns, self-loops have been removed, as suggested [34]. Finally, we obtain a weighted directed network characterized by a weighted adjacency matrix $W = \{w_{ij}\}, i, j \in [1, 2^n]$. The matrix W fulfils the normalization $\sum_{i,j}^{2^n} w_{ij} = 1$. Here, based on W, the regularity of the order pattern transition properties is quantified by the Shannon entropy $\mathcal{H}_T$, which is

$$\mathcal{H}_T = -\sum_{i,j=1}^{2^n} w_{ij} \log_2 w_{ij}, \tag{4}$$

where the sum runs over all possible 2^{2n} transitions. In a full analogy to $\mathcal{H}_O$, for an n-dimensional independent identical distributed stochastic process, one obtains the largest entropy $\mathcal{H}_T = 2n$.

Both measures have been demonstrated to show the capability of capturing different bifurcation transition scenarios. In the examples in this work, we show that $\mathcal{H}_O$ and $\mathcal{H}_T$ are sensitive to PS.

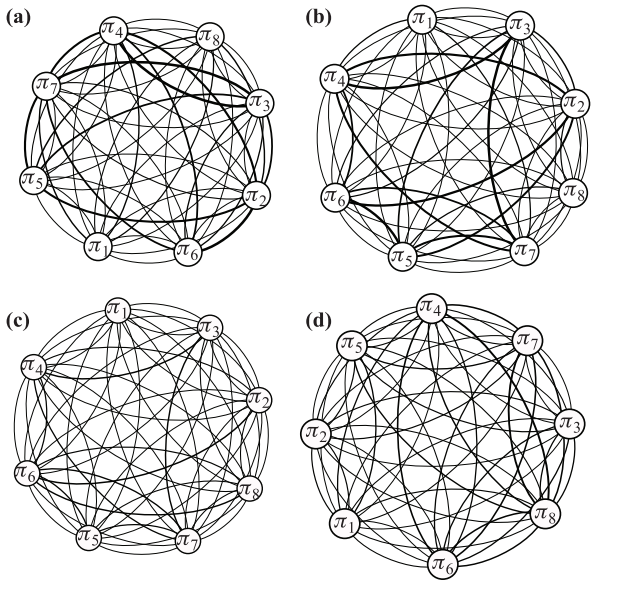

Fig. 2 Ordinal pattern transition network for **(a)** a single stochastic process. **(b)** A COPT for two coupled stochastic processes, **(c)** an alternative version of COPT, and **(d)** a JOPT. For better visualization, the arrows of links are suppressed.

3 Detecting transitions to PS

3.1 Preliminaries on PS

In this section, traditional measures characterizing PS are briefly reviewed; more historical details can be found in [35, 43, 44]. PS is characterized by the phase locking $|m\phi_1 - n\phi_2| < C$, where m, n, and C are constants and $\phi_1(t)$ and $\phi_2(t)$ are phases of the two oscillators.

In the case of two coupled Rössler oscillators, we can easily compute phases using $\phi_1(t) = \arctan y_1(t)/x_1(t)$ and $\phi_2(t) = \arctan y_2(t)/x_2(t)$ because the systems are in phase-coherent regimes. In addition, m and n are often chosen as 1 because 1:1 phase synchronization is frequently observed. Equivalently, the phase locking is characterized as the average frequency mismatch drops to zero, i.e., $\Delta\Omega = 0$, where $\Delta\Omega = \Omega_1 - \Omega_2$ and $\Omega_{1,2} = \frac{1}{2\pi}\left\langle \frac{d\phi_{1,2}(t)}{dt} \right\rangle$, where $\langle\cdot\rangle$ is an average over time T. PS has been related to the spectrum of Lyapunov exponents [45], and it is characterized by the transition of the Lyapunov exponent from zero to negative values [35].

3.2 Unidirectional coupling schemes

In the coupled Rössler systems [Eqs. (1)], PS can be achieved by applying the unidirectional coupling scheme $\kappa_1 = 0$ and relative small frequency mismatch Δ between ω_1 and ω_2 [41]. More specifically, we choose $\Delta = 0.02$ and $(\omega_1, \omega_2) = (0.98, 1.02)$. Note that in this model, generalized synchronization is obtained for relative large values of $\Delta = 0.2$, which leads to $(\omega_1, \omega_2) = (0.8, 1.2)$. The interrelationship between PS and generalized synchronization has been systematically investigated in Ref. [41].

We first showed in Fig. 3 that the variations of network measures of COPTs depend on the coupling parameters κ_2 ($\kappa_1 = 0$). When increasing the coupling κ_2, the frequencies of ordinal patterns $\mathcal{F}(\pi_i)$ experience relative large variations [Figs. 3(a)]. In consequence, both $\mathcal{H}_T$ and $\mathcal{H}_O$ show fast decays to small values when the coupling threshold κ_2 passes the transition values [as highlighted by vertical dashed lines in Fig. 3(b)]. The transition point to PS has been validated by the average rotation frequencies of Ω_1 and Ω_2 because they are locked to the same value at $\kappa_2 = 0.07$. We choose three representative coupling values, $\kappa_2 = 0.04, 0.08$, and 0.12, to show the structural variations of the corresponding COPTs in Figs. 5(a–c). In the non-synchrony regime ($\kappa_2 = 0.04$), the transitions between ordinal patterns and their frequencies are rather random [Fig. 5(a)]. As the coupling increases to just above the critical value $\kappa_2 = 0.08$, a dominant (more deterministic) transition route emerges [Fig. 5(b)]. When PS is achieved for large $\kappa_2 = 0.12$, more missing patterns are observed [Fig. 5(c)]. We note that the different pattern definitions are used between the ordinal transition network for a single chaotic Rössler system, as shown in Fig. 1(a), and the COPT for two coupled systems [Fig. 5(c)]. Unidirectional coupling leads to the entrainment of the response to the drive system, which yields the same ordinal partitions for phase space as the drive. Because of the continuity of phase space trajectory, we observe a similar deterministic transition route between phase space partitions as for a single system.

Concerning network measures from JOPTs, we have obtained rather similar results, as shown in Fig. 4. Three representative JOPTs on the route to PS are illustrated in Figs. 5(d–f). As the coupling strength increases, the random transitions between patterns become more deterministic, yielding more missing patterns.

Based on the results of Figs. 3, 4, and 5, we conclude that $\mathcal{H}_O$ and $\mathcal{H}_T$ can effectively capture the transitions to PS. However, the detailed variations of particular patterns remain unclear during the transitions to PS. In

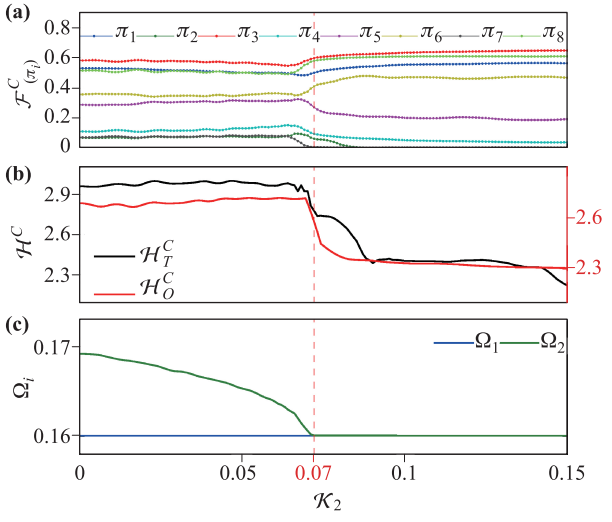

Fig. 3 Network measures of COPTs versus the coupling strength κ_2 for two unidirectionally coupled Rössler systems ($\kappa_1 = 0$, $\Delta = 0.02$, i.e., $\omega_1 = 0.98$ and $\omega_2 = 1.02$ in Eqs. (1). **(a)** Frequencies of ordinal patterns $\mathcal{F}(\pi_i)$ with increasing coupling strength κ_2. **(b)** $\mathcal{H}_O$ and $\mathcal{H}_T$. **(c)** The average rotation frequencies Ω_1 and Ω_2. In all cases, vertical dashes highlight the critical synchronization transition thresholds $\kappa_2 = 0.07$ [41]. Superscripts C denote COPTs.

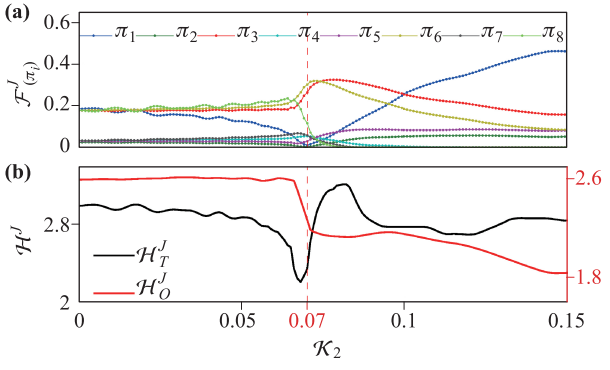

Fig. 4 Network measures of JOPTs versus the coupling strength κ_2 for two unidirectionally coupled Rössler systems ($\kappa_1 = 0$). **(a)** Frequencies of ordinal patterns with increasing coupling strength. **(b)** $\mathcal{H}_O$ and $\mathcal{H}_T$. Superscripts J denoted JOPTs.

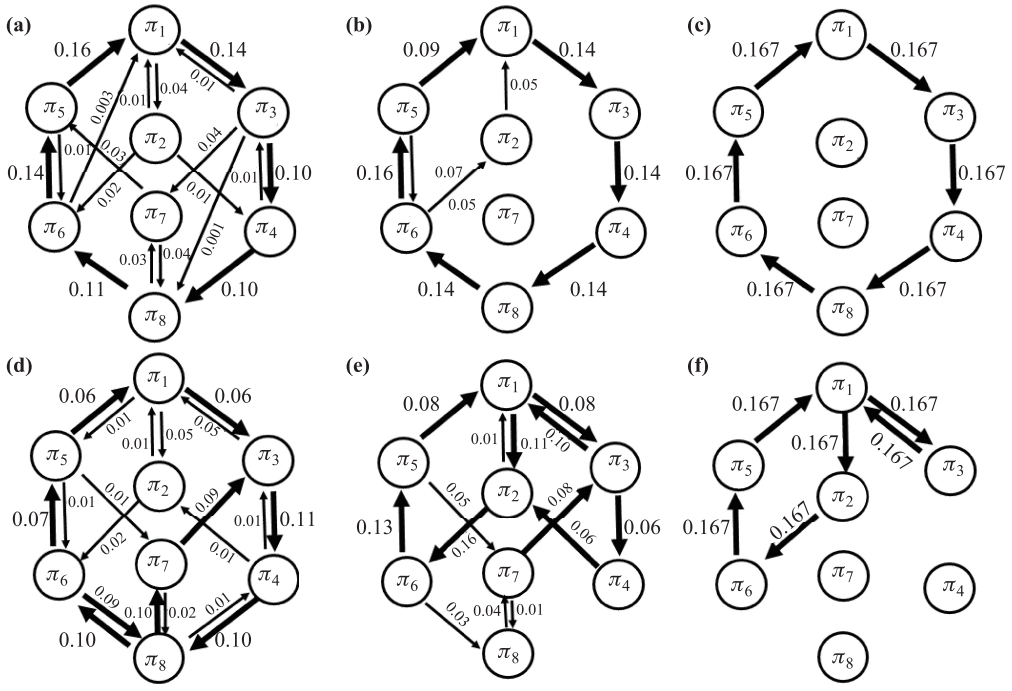

Fig. 5 Network illustrations for COPTs **(a–c)** and JOPTs **(e–f)**. (a, d) $\kappa_2 = 0.04$, (b, e) $\kappa_2 = 0.08$, and (c, f) $\kappa_2 = 0.12$. Directions of pattern transitions and the corresponding frequencies are indicated by arrows and the values on links.

other words, we have to investigate the details of the appearance or disappearance of each ordinal patterns [as shown in Fig. 3(a) and Fig. 4(a)] because some of the patterns become suppressed, which provides further evidence for characterizing the synchronization dynamics.

It is easy to understand the occurrences of missing patterns on the transition routes to synchronization. As the coupling strength is increased during the synchronization transitions, the high-dimensional coupled systems are constrained to a lower-dimensional synchronization manifold, which means that the determinism of the system is increased. Consequently, both the frequencies of order patterns and the transitions between different patterns become more inhomogeneous. Therefore, we compute the missing probability (frequency) of each pattern while varying the coupling strengths.

3.3 Bidirectional coupling schemes

In this section, we implement a bidirectional coupling scheme when choosing $\kappa_1 = \kappa_2 = \kappa$. In addition, we show the transition to synchronization in a two-dimensional parameter space of coupling strength $\kappa \in [0.0, 1.2]$ and natural frequency mismatch $\Delta \in [-0.04, 0.04]$. We choose this particular range of parameters because there are different routes of chaos-chaos, chaos-period-chaos transitions to synchronizations [42]. This space (Δ, κ) is further divided into 800×1200 grid points with equal step sizes. For each parameter combination, we integrate the ODEs with the same strategy as described in Section 2.1 to obtain time series for the coupled system. Then, we construct both COPTs and JOPTs.

First, we show the average frequency mismatches $\Delta\Omega$ in the parameter space (Δ, κ), where PS is characterized by the well-known Arnold tongue [35], as shown in Fig. 6(a). PS are observed inside this Arnold tongue, while no PS occurs outside this region. We further validate these results by computing the Lyapunov spectrum of the whole system based on Eqs. (1) [Fig. 6(b)]. We note that it may not be possible to distinguish the tip of the Arnold tongue only by considering the sum of positive Lyapunov exponents because of the non-hyperbolic property of the coupled 6-dimensional system. One interesting structure inside the Arnold tongue is the periodic region close to $0.03 < \kappa < 0.04$ (like two eyes), which has been reported in Ref. [42]. It is often claimed that all transitions between different types of synchronization are related to the changes in the Lyapunov spectrum [45]. In particular, for low values of the coupling strength, the following configuration for the coupled 6-dimension system occurs: $\{\lambda_1 > 0, \lambda_2 > 0, \lambda_3 \sim 0, \lambda_4 \sim 0, \lambda_5 < 0, \lambda_6 < 0\}$. Increasing the coupling strength, PS is achieved when λ_4 becomes negative. If the coupling strength is further increased, generalized synchronization is obtained as $\lambda_2 \sim 0$ and $\lambda_3 < 0$. However, for intermediate coupling strengths and relative large frequency mismatches, the spectrum of Lyapunov exponents has limited power to explain the weak correlations outside

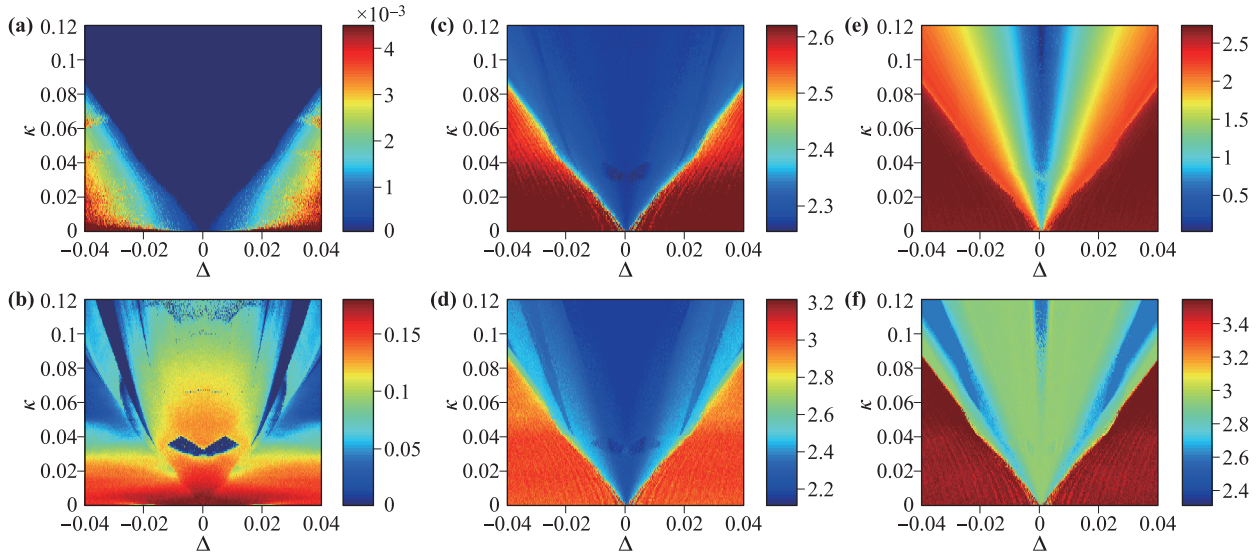

Fig. 6 Two parameter space (frequency mismatches Δ and coupling strength $\kappa_1 = \kappa_2 = \kappa$), which is color coded by the network statistics obtained from COPTs and JOPTs. **(a)** The difference of the mean frequencies $\Delta\Omega = \Omega_1 - \Omega_2$, **(b)** the sum of non-negative Lyapunov exponents of the coupled system. COPTs: **(c)** $\mathcal{H}_O$, **(d)** $\mathcal{H}_T$, and JOPTs: **(e)** $\mathcal{H}_O$, **(f)** $\mathcal{H}_T$.

the Arnold tongue, although the phases are not locked [42].

Figures 6(c–f) show the parameter space color coded by the entropy values $\mathcal{H}_O$ and $\mathcal{H}_T$, which are calculated from the respective COPTs and JOPTs. The outer borders of the Arnold tongue have been successfully captured by $\mathcal{H}_O$ and $\mathcal{H}_T$, compared with the average frequency mismatch plot [Fig. 6(a)]. More importantly, all these entropy values are able to capture the tip of the Arnold tongue; however, the spectrum of Lyapunov exponents does not [Fig. 6(b)]. Therefore, Figs. 6(c–f) provide important complementary information to the sum of the positive Lyapunov exponents.

Inside the Arnold tongue, however, these entropy values drop to small values, presenting more intricate gradient structures. Nevertheless, the entropy values do not convincingly show the periodic region close to $0.03 < \kappa < 0.04$, except for the case of $\mathcal{H}_T$ computed from COPTs. This is because $\mathcal{H}_O$ and $\mathcal{H}_T$ are averaged over all patterns.

To more clearly illustrate the gradient structures inside and on the edge of the Arnold tongue, we plot the missing (failure) probabilities of individual ordinal patterns in the space (Δ, κ). For one combination of parameter pair (Δ, κ), we run $n = 200$ simulations of random initial conditions. The COPT and JOPT have been reconstructed for each realization of $N = 800000$ time points, and the frequency plots of ordinal patterns have been obtained. Furthermore, this ensemble of independent realizations results in a failure with probability $p_{\pi_i} = 1$ if pattern π_i is missing and a success with probability $p_{\pi_i} = 0$ if π_i is observed.

In the case of COPTs, Fig. 7 shows that π_1, π_3, π_4, π_5, π_6, and π_8 are observed patterns for the entire range of parameters considered. In addition, we find that pattern π_2 is completely not observed in the Arnold tongue, and the disappearance of π_2 sharply determines the outer border. In addition, pattern π_7 plays a key role in forming the periodic eye structures inside the Arnold tongue. In the case of JOPTs, Fig. 8 shows that patterns π_1, π_2, π_3, and π_5 do appear in the majority area of the parameter space. Again, the disappearance of patterns π_7 and π_8 determine sharply the outer borders of the Arnold tongue, while the inside structures are determined by π_4 and π_6.

4 Conclusions

In summary, we propose to construct cross and joint ordinal pattern transition networks from multivariate time series, which has been particularly applied to analyze synchronization transitions. Note that a COPT and JOPT are two slightly different ways to construct networks from time series, providing complementary information. The ordinal patterns of a COPT are defined by considering the signs of the difference of $\Delta\boldsymbol{x}_1 - \Delta\boldsymbol{x}_2$ between two subsystems. In contrast, the ordinal patterns of a JOPT are defined by the signs of the product of $\Delta\boldsymbol{x}_1 \cdot \Delta\boldsymbol{x}_2$. It is certain that the amplitudes of oscillations of different variables directly influence the definition of a COPT. However, the amplitudes are not important for a JOPT because only the signs of the product are considered. In addition, it is straightforward to generalize the

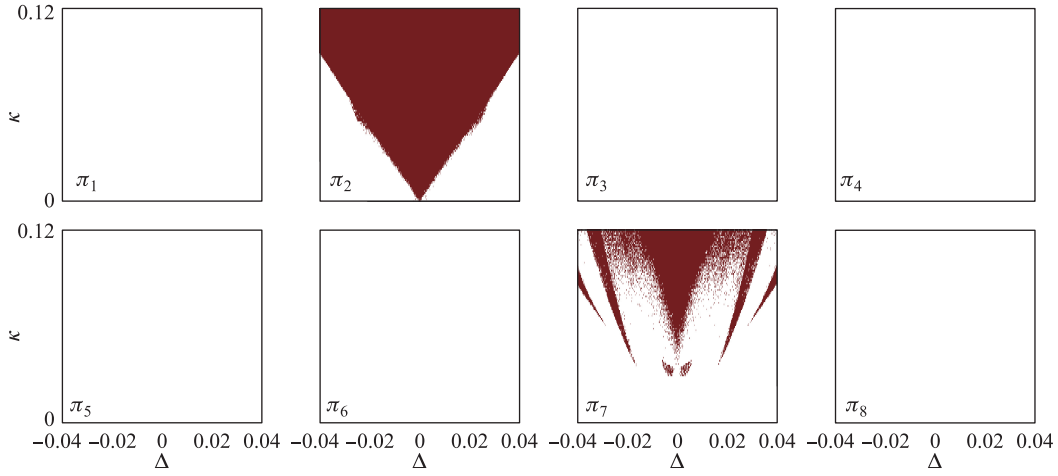

Fig. 7 Two parameter space (Δ, κ) highlighted by the missing (failure) probability of individual patterns obtained from COPTs. Note that $\pi_1, \pi_3, \pi_4, \pi_5, \pi_6$, and π_8 are observed for the entire range of parameters (white areas). Red regions correspond to the missing probabilities of patterns, which show that π_2 primarily captures the outer borders of the Arnold tongue and π_7 captures the inside structures, including two eye-like periodic regions.

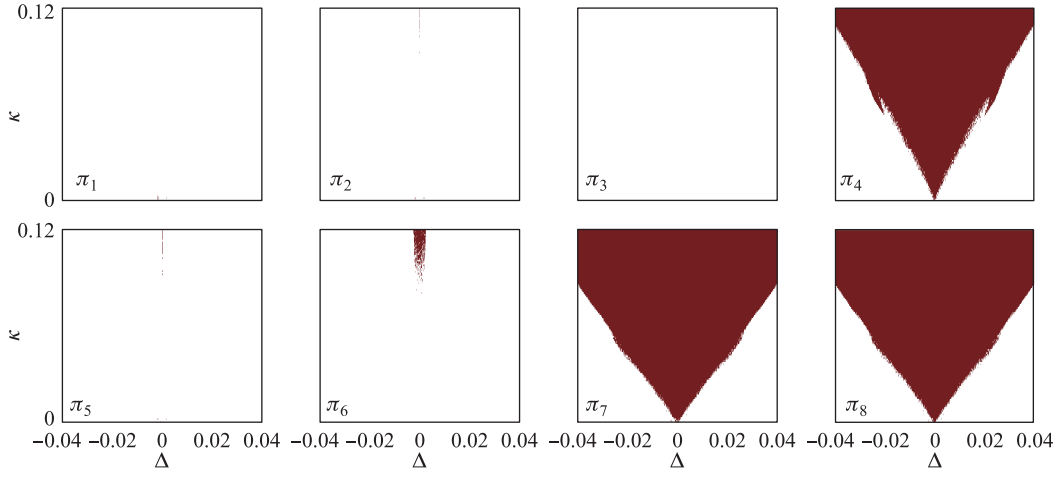

Fig. 8 Two parameter space (Δ, κ) highlighted by the missing (failure) probability of the individual pattern obtained from JOPTs. Note that π_1, π_2, π_3, and π_5 are observed for the majority area of the parameter space (white areas). The red regions correspond to the missing probabilities of patterns, showing that π_7 and π_8 capture the outer borders, while π_4 and π_6 affect the inside structures of the Arnold tongue.

ideas of JOPTs from two to three (or even n) coupled subsystems with an extended number of pattern definitions. We plan to further generalize the ideas of JOPTs to multilayer or multiplex networks for time series analysis. However, constructing a COPT for three coupled subsystems remains a challenge.

Based on the cross and joint ordinal pattern transition networks, we propose two entropy measures to characterize the resulting networks. Namely, $\mathcal{H}_O$ is calculated from the frequencies of each pattern, and $\mathcal{H}_T$ is obtained from the transition frequencies between any pair of patterns. Our results show that both $\mathcal{H}_O$ and $\mathcal{H}_T$ successfully track the critical coupling threshold to phase synchronization. The applications of our method to generalization synchronization analysis is a more challenging task and will be a subject for future work [43].

In the two parameter space of (Δ, κ), both entropy measures capture the tip of the Arnold tongue successfully, providing complementary information to the traditional measure of Lyapunov exponents. To show the intricate structures inside the Arnold tongue, our results suggest that we should study the missing probability of each pattern separately, instead of relying on the global measures of $\mathcal{H}_O$ and $\mathcal{H}_T$. This is because individual patterns show different sensitivities to dynamic transitions. In particular, we have observed particular missing pat-

terns that correspond to the outer borders and the inner structures in the parameter space.

In addition to synchronization analysis based on real time series, identifying the driver-response relationship remains an interesting topic, especially indirect identification from direct coupling directions [46–49]. From the viewpoint of ordinal patterns, it is possible to combine ordinal recurrence plots [50] and cross and joint ordinal partition transition network approaches to tackle this problem. More importantly, we plan to address the statistical significance of the coupling directions for real time series data.

Acknowledgements This work was in part financially sponsored by the Natural Science Foundation of Shanghai (Grant No. 17ZR1444800 and 18ZR1411800).

References

1. R. V. Donner, M. Small, J. F. Donges, N. Marwan, Y. Zou, R. Xiang, and J. Kurths, Recurrence-based time series analysis by means of complex network methods, *Int. J. Bifurcat. Chaos* 21(04), 1019 (2011)
2. R. V. Donner, Y. Zou, J. F. Donges, N. Marwan, and J. Kurths, Recurrence networks – A novel paradigm for nonlinear time series analysis, *New J. Phys.* 12(3), 033025 (2010)
3. N. Marwan, J. F. Donges, Y. Zou, R. V. Donner, and J. Kurths, Complex network approach for recurrence analysis of time series, *Phys. Lett. A* 373(46), 4246 (2009)
4. L. Lacasa, B. Luque, F. Ballesteros, J. Luque, and J. C. Nuno, From time series to complex networks: The visibility graph, *Proc. Natl. Acad. Sci. USA* 105(13), 4972 (2008)
5. J. Zhang and M. Small, Complex network from pseudoperiodic time series: Topology versus dynamics, *Phys. Rev. Lett.* 96(23), 238701 (2006)
6. Y. Yang and H. Yang, Complex network-based time series analysis, *Physica A* 387(5–6), 1381 (2008)
7. J. F. Donges, R. V. Donner, M. H. Trauth, N. Marwan, H. J. Schellnhuber, and J. Kurths, Nonlinear detection of paleoclimate-variability transitions possibly related to human evolution, *Proc. Natl. Acad. Sci. USA* 108(51), 20422 (2011)
8. Y. Zou, R. V. Donner, M. Wickramasinghe, I. Z. Kiss, M. Small, and J. Kurths, Phase coherence and attractor geometry of chaotic electrochemical oscillators, *Chaos* 22(3), 033130 (2012)
9. Z. K. Gao, W. D. Dang, Y. X. Yang, and Q. Cai, Multiplex multivariate recurrence network from multichannel signals for revealing oil-water spatial flow behavior, *Chaos* 27(3), 035809 (2017)
10. J. B. Elsner, T. H. Jagger, and E. A. Fogarty, Visibility network of united states hurricanes, *Geophys. Res. Lett.* 36(16), L16702 (2009)
11. Y. Zou, M. Small, Z. Liu, and J. Kurths, Complex network approach to characterize the statistical features of the sunspot series, *New J. Phys.* 16(1), 013051 (2014)
12. Y. Zou, R. Donner, N. Marwan, M. Small, and J. Kurths, Long-term changes in the north-south asymmetry of solar activity: A nonlinear dynamics characterization using visibility graphs, *Nonlinear Process. Geophys.* 21(6), 1113 (2014)
13. R. Zhang, Y. Zou, J. Zhou, Z. K. Gao, and S. Guan, Visibility graph analysis for re-sampled time series from auto-regressive stochastic processes, *Commun. Nonlinear Sci. Numer. Simul.* 42, 396 (2017)
14. Z. Czechowski, M. Lovallo, and L. Telesca, Multifractal analysis of visibility graph-based Ito-related connectivity time series, *Chaos* 26(2), 023118 (2016)
15. C. Zhang, Y. Chen, and G. Hu, Network reconstructions with partially available data, *Front. Phys.* 12(3), 128906 (2017)
16. Z. Q. Jiang, Y. H. Yang, G. J. Wang, and W. X. Zhou, Joint multifractal analysis based on wavelet leaders, *Front. Phys.* 12(6), 128907 (2017)
17. R. V. Donner, J. Heitzig, J. F. Donges, Y. Zou, N. Marwan, and J. Kurths, The geometry of chaotic dynamics — A complex network perspective, *Eur. Phys. J. B* 84(4), 653 (2011)
18. M. McCullough, M. Small, T. Stemler, and H. H. C. Iu, Time lagged ordinal partition networks for capturing dynamics of continuous dynamical systems, *Chaos* 25(5), 053101 (2015)
19. C. W. Kulp, J. M. Chobot, H. R. Freitas, and G. D. Sprechini, Using ordinal partition transition networks to analyze ECG data, *Chaos* 26(7), 073114 (2016)
20. C. W. Kulp, J. M. Chobot, B. J. Niskala, and C. J. Needhammer, Using forbidden ordinal patterns to detect determinism in irregularly sampled time series, *Chaos* 26(2), 023107 (2016)
21. M. McCullough, K. Sakellariou, T. Stemler, and M. Small, Counting forbidden patterns in irregularly sampled time series (i): The effects of under-sampling, random depletion, and timing jitter, *Chaos* 26(12), 123103 (2016)
22. K. Sakellariou, M. McCullough, T. Stemler, and M. Small, Counting forbidden patterns in irregularly sampled time series (ii): Reliability in the presence of highly irregular sampling, *Chaos* 26(12), 123104 (2016)
23. C. Bandt and B. Pompe, Permutation entropy: A natural complexity measure for time series, *Phys. Rev. Lett.* 88(17), 174102 (2002)
24. U. Parlitz, H. Suetani, and S. Luther, Identification of equivalent dynamics using ordinal pattern distributions, *Eur. Phys. J. S.T.* 222(2), 553 (2013)
25. J. M. Amigó, K. Keller, and V. A. Unakafova, Ordinal symbolic analysis and its application to biomedical recordings, *Phil. Trans. R. Soc. A* 373(2034), 20140091 (2014)

26. F. Takens, Detecting strange attractors in turbulence, in: D. Rand and L.-S. Young (Eds.), Dynamical Systems and Turbulence, Warwick 1980, Vol. 898 of Lecture Notes in Mathematics, Springer, New York, 1981, pp 366–381
27. H. Kantz and T. Schreiber, Nonlinear Time Series Analysis, 2nd Ed., Cambridge: Cambridge University Press, 2004
28. J. M. Amigó, S. Zambrano, and M. A. F. Sanju'an, True and false forbidden patterns in deterministic and random dynamics, *Europhys. Lett.* 79(5), 50001 (2007)
29. J. M. Amigó, S. Zambrano, and M. A. F. Sanju'an, Combinatorial detection of determinism in noisy time series, *Europhys. Lett.* 83(6), 60005 (2008)
30. O. A. Rosso, L. C. Carpi, P. M. Saco, M. G. Ravetti, H. A. Larrondo, and A. Plastino, The Amig'o paradigm of forbidden/missing patterns: A detailed analysis, *Eur. Phys. J. B* 85(12), 419 (2012)
31. O. A. Rosso, L. C. Carpi, P. M. Saco, M. Gómez Ravetti, A. Plastino, and H. A. Larrondo, Causality and the entropy-complexity plane: Robustness and missing ordinal patterns, *Physica A* 391(1–2), 42 (2012)
32. C. W. Kulp and L. Zunino, Discriminating chaotic and stochastic dynamics through the permutation spectrum test, *Chaos* 24(3), 033116 (2014)
33. A. Politi, Quantifying the dynamical complexity of chaotic time series, *Phys. Rev. Lett.* 118(14), 144101 (2017)
34. J. Zhang, J. Zhou, M. Tang, H. Guo, M. Small, and Y. Zou, Constructing ordinal partition transition networks from multivariate time series, *Sci. Rep.* 7(1), 7795 (2017)
35. A. Pikovsky, M. Rosenblum, and J. Kurths, Synchronization – A Universal Concept in Nonlinear Sciences, Cambridge University Press, 2001
36. G. V. Osipov, B. Hu, C. Zhou, M. V. Ivanchenko, and J. Kurths, Three types of transitions to phase synchronization in coupled chaotic oscillators, *Phys. Rev. Lett.* 91(2), 024101 (2003)
37. J. Zhang, Y. Z. Yu, and X. G. Wang, Synchronization of coupled metronomes on two layers, *Front. Phys.* 12(6), 120508 (2017)
38. H. B. Chen, Y. T. Sun, J. Gao, C. Xu, and Z. G. Zheng, Order parameter analysis of synchronization transitions on star networks, *Front. Phys.* 12(6), 120504 (2017)
39. X. Huang, J. Gao, Y. T. Sun, Z. G. Zheng, and C. Xu, Effects of frustration on explosive synchronization, *Front. Phys.* 11(6), 110504 (2016)
40. L. M. Ying, J. Zhou, M. Tang, S. G. Guan, and Y. Zou, Mean-field approximations of fixation time distributions of evolutionary game dynamics on graphs, *Front. Phys.* 13(1), 130201 (2018)
41. Z. Zheng and G. Hu, Generalized synchronization versus phase synchronization, *Phys. Rev. E* 62(6), 7882 (2000)
42. M. C. Romano, M. Thiel, J. Kurths, and W. von Bloh, Multivariate recurrence plots, *Phys. Lett. A* 330(3–4), 214 (2004)
43. L. M. Pecora and T. L. Carroll, Synchronization of chaotic systems, *Chaos* 25(9), 097611 (2015)
44. S. Boccaletti, J. Kurths, G. Osipov, D. Valladares, and C. Zhou, The synchronization of chaotic systems, *Phys. Rep.* 366(1–2), 1 (2002)
45. M. G. Rosenblum, A. S. Pikovsky, and J. Kurths, From phase to lag synchronization in coupled chaotic oscillators, *Phys. Rev. Lett.* 78(22), 4193 (1997)
46. M. G. Rosenblum and A. S. Pikovsky, Detecting direction of coupling in interacting oscillators, *Phys. Rev. E* 64(4), 045202 (2001)
47. M. C. Romano, M. Thiel, J. Kurths, and C. Grebogi, Estimation of the direction of the coupling by conditional probabilities of recurrence, *Phys. Rev. E* 76(3), 036211 (2007)
48. J. Nawrath, M. C. Romano, M. Thiel, I. Z. Kiss, M. Wickramasinghe, J. Timmer, J. Kurths, and B. Schelter, Distinguishing direct from indirect interactions in oscillatory networks with multiple time scales, *Phys. Rev. Lett.* 104(3), 038701 (2010)
49. Y. Zou, M. C. Romano, M. Thiel, N. Marwan, and J. Kurths, Inferring indirect coupling by means of recurrences, *Int. J. Bifurcat. Chaos* 21(04), 1099 (2011)
50. A. Groth, Visualization of coupling in time series by order recurrence plots, *Phys. Rev. E* 72(4), 046220 (2005)